Geophysical Research Letters

RESEARCH LETTER
10.1029/2023GL104797

Key Points:

- High pressure-temperature single-crystal elasticity measurements of jadeite are conducted by Brillouin spectroscopy
- Jadeite is among the seismically fastest phases in the Earth's upper mantle
- Delaminated lower crust can help explain the fast seismic anomalies under cratons

Supporting Information:

Supporting Information may be found in the online version of this article.

Correspondence to:

J. S. Zhang and M. Hao,
jinzhang@tamu.edu;
mhao@carnegiescience.edu

Citation:

Hao, M., Zhou, W.-Y., Dera, P., Schmandt, B., Zhang, D., & Zhang, J. S. (2024). Fast seismic anomalies under continents explained by the delaminated lower continental crust—Implications from high pressure-temperature elasticity of jadeite. *Geophysical Research Letters*, *51*, e2023GL104797. https://doi.org/10.1029/2023GL104797

Received 8 JUN 2023
Accepted 16 APR 2024

Author Contributions:

Conceptualization: Brandon Schmandt, Jin S. Zhang
Formal analysis: Ming Hao
Funding acquisition: Jin S. Zhang
Investigation: Ming Hao, Wen-Yi Zhou, Przemyslaw Dera, Dongzhou Zhang
Methodology: Ming Hao, Jin S. Zhang
Resources: Jin S. Zhang
Software: Wen-Yi Zhou
Supervision: Jin S. Zhang
Validation: Brandon Schmandt
Visualization: Ming Hao, Wen-Yi Zhou
Writing – original draft: Ming Hao, Jin S. Zhang

Fast Seismic Anomalies Under Continents Explained by the Delaminated Lower Continental Crust—Implications From High Pressure-Temperature Elasticity of Jadeite

Ming Hao[1,2,3], Wen-Yi Zhou[1,2,4], Przemyslaw Dera[5], Brandon Schmandt[1], Dongzhou Zhang[5,6], and Jin S. Zhang[4]

[1]Department of Earth and Planetary Sciences, University of New Mexico, Albuquerque, NM, USA, [2]Institute of Meteoritics, University of New Mexico, Albuquerque, NM, USA, [3]Earth and Planets Laboratory, Carnegie Institution for Science, Washington, DC, USA, [4]Department of Geology and Geophysics, Texas A&M University, College Station, TX, USA, [5]Hawaii Institute of Geophysics and Planetology, University of Hawaii at Manoa, Honolulu, HI, USA, [6]Argonne National Laboratory, GeoSoilEnviroCARS, University of Chicago, Argonne, IL, USA

Abstract Seismic tomography has shown that the shear wave velocities (Vs) under continents, especially under cratons, are extremely fast at 100–200 km depth, which is difficult to explain by low temperatures or high Mg#. Alternatively, delaminated eclogitic lower continental crust has been proposed to account for these fast seismic anomalies. However, the thermoelastic properties of jadeite which constitutes up to 60–80 mol% of clinopyroxene in the potentially delaminated lower continental crust are not well constrained. In this study, we measured the single-crystal elasticity of jadeite by Brillouin spectroscopy under simultaneous high pressure and temperature conditions for the first time. We found that the temperature dependence of Vs of jadeite is extremely small if not negligible. The seismic velocities of the potentially delaminated lower continental crusts were subsequently modeled and found to match the widely observed fast seismic anomalies under cratons between 100 and 200 km depth.

Plain Language Summary The seismic wave velocity variation images show the potential composition and temperature heterogeneities inside the Earth. Fast shear wave velocities (~7% higher than the global average) have been observed under continents at 100–200 km depths. A candidate explanation of this fast shear wave velocity anomaly is the existence of delaminated eclogitic lower continental crust. However, due to the lack of knowledge of the thermoelastic properties of clinopyroxene, which is the dominant mineral phase (up to 60 vol%) in delaminated eclogitic lower continental crust, evaluation of this hypothesis is difficult. Clinopyroxene in the potentially delaminated lower continental crust is jadeite-rich (up to 60–80 mol%) due to its high Na content (2.5–3.5 wt%). In this study, we report single-crystal elasticity of jadeite at high pressure-temperature conditions. We found the Vs of jadeite is much higher than all the other major upper mantle minerals under upper mantle conditions. The calculated seismic velocities of the potentially delaminated lower continental crusts could easily account for the fast shear wave anomalies observed under cratons.

1. Introduction

Global seismic shear wave velocity tomography models (e.g., SEMum2, GLAD-M25, and DR2020s) have suggested an elevated Vs (up to 4.8–4.9 km/s) under continents, especially under continental cratons (e.g., North American Cratons, Australian Cratons, and Scandinavian Cratons) at ~100–200 km depth (Debayle et al., 2020; French et al., 2013; Lei et al., 2020). Popular explanations for these fast seismic anomalies include low temperatures under stable cratons (Dalton & Faul, 2010; Reston & Morgan, 2004), high Mg#s resulting from chemical depletion (Dalton & Faul, 2010; Lee, 2003; Schutt & Lesher, 2006), higher olivine fractions (James et al., 2004), and the existence of diamond (Garber et al., 2018). As an alternative explanation, the potentially delaminated lower continental crust (PDLCC) has been proposed to be responsible for the fast seismic anomalies under continents as well (e.g., Wang et al., 2016). Under high pressure-temperature conditions, the basaltic lower continental crust transforms into intrinsically fast and dense eclogitic materials. The gravitationally unstable eclogitic lower crust can then delaminate and sink into the Earth's upper mantle (Kay & Kay, 1993).

To evaluate these hypotheses, especially the existence of PDLCC, for explaining the fast seismic anomalies under cratons, the high pressure-temperature composition-dependent elastic properties of relevant minerals are needed.

Writing – review & editing: Ming Hao, Wen-Yi Zhou, Przemyslaw Dera, Brandon Schmandt, Dongzhou Zhang, Jin S. Zhang

Under high pressure-temperature conditions, the eclogitic PDLCC contains up to 60 vol% clinopyroxenes. Due to the high Na content of the lower continental crust (Rudnick & Fountain, 1995), the jadeite component in the PDLCC clinopyroxene is up to 60–80 mol%. Therefore, the thermoelastic properties of jadeite under high pressure-temperature conditions are crucial to constrain the seismic properties of PDLCC. However, the elastic properties of jadeite have not been measured under simultaneous high pressure-temperature conditions (Hao et al., 2020; Kawai & Tsuchiya, 2010; Walker, 2012). In this study, we performed single-crystal Brillouin spectroscopy experiments on jadeite at various pressures (up to 16.7 GPa) and temperatures (up to 700 K) at University of New Mexico (UNM). We also conducted phase equilibrium calculations with Perple_X using the most recent thermodynamic database from Stixrude and Lithgow-Bertelloni (2022) to obtain the mineral proportions and compositions of the PDLCC under mantle conditions. Finally, combining the Perple_X calculation results with the experimentally determined thermoelastic properties of relevant minerals in PDLCC, we modeled the seismic properties of PDLCC from 30 to 500 km depth and evaluated different hypotheses for explaining the fast seismic anomalies under continents at 100–200 km depth.

2. Materials and Methods

2.1. High Pressure-Temperature Brillouin Experiments

The jadeite crystals used in this study were selected from a natural jadeitite sample that has been used for the measurements in Hao et al. (2019, 2020). The chemical composition, $Na_{0.954}Mg_{0.021}Ca_{0.029}Fe_{0.019}Al_{0.966}Si_{2.002}O_6$, was determined by the JEOL 8200 Electron Microprobe at UNM (Text S1 in Supporting Information S1). The hand-picked inclusion-free crystals were polished into platelets with 15–20 μm thickness. Then the scratch-free crystals were broken into small pieces with diameters of 40–50 μm and loaded into diamond anvil cells (DACs). The plane normals of the three selected and polished crystals were (−0.692, −0.714, 0.106), (0.116, 0.993, −0.021), and (−0.896, −0.338, 0.289) and determined at Sector 13-BMC, GeoSoilEnviroCARS (GSECARS), Advanced Photon Source (APS), Argonne National Laboratory (ANL) and the X-ray Atlas Diffraction Lab, University of Hawai'i at Mānoa (Text S1 in Supporting Information S1). The first two crystals were used in Hao et al. (2020), while the third crystal with plane normal (−0.896, −0.338, 0.289) was newly prepared and not used in Hao et al. (2020). As shown in Figure S1 in Supporting Information S1, the measured Vp and Vs of the selected three jadeite crystals are enough to constrain the 13 independent single-crystal elastic moduli (C_{ij}s) of jadeite.

450 μm culet diamonds were glued on WC seats with 90° optical opening and installed inside BX90 DACs for high pressure-temperature Brillouin experiments. ~280 μm diameter holes were drilled into the pre-indented 50–55 μm thick rhenium gaskets and served as sample chambers. Neon was gas-loaded into sample chambers as pressure transmitting medium at GSECARS, APS, ANL (Rivers et al., 2008). Two ruby spheres were loaded into the sample chamber as pressure markers (Text S2 in Supporting Information S1; Datchi et al., 2007; Mao et al., 1986). The pressure uncertainties were determined from the four ruby fluorescence pressure readings before and after the experiments. Pt wires were twined on pyrophyllite as heaters, and two K-type thermocouples were placed in contact with the diamond and near the culet for temperature measurements. The differences between the temperature readings from two thermocouples were less than 10 K.

A single-mode 300 mW 532 nm solid-state laser was used for Brillouin spectroscopy experiments at UNM. A standard silica glass (Corning 7980) was used to calibrate the scattering angle as 50.6(1)° under symmetric forward scattering geometry. The three jadeite crystals with known plane normal were measured at 13 different Chi angles (0°, 30°, 60°, 90°, 120°, 150°, 180°, 195°, 225°, 255°, 285°, 315°, 345°) to reduce the geometrical errors. Figure S2 in Supporting Information S1 shows a typical Brillouin spectrum.

2.2. Perple_X Calculations

To calculate the mineral proportions and compositions of the PDLCC under high pressure-temperature conditions, we used Perple_X software (Connolly, 2009) with the most recent thermodynamic database from Stixrude and Lithgow-Bertelloni (2022), which offers improved constraints for assemblages involving multiple components and phases, considering phase transformation and chemical exchange effects. The starting compositions of lower continental crust under different tectonic settings (Platform Shield, Mesozoic-Cenozoic Contractions, Mesozoic-Cenozoic Extensions, Continental Arcs, and Active Rifts) are obtained from Rudnick and Fountain (1995) (Table S1 in Supporting Information S1). We calculated the phase proportions and chemical

compositions of individual mineral phases from 30 to 500 km depth. It is worth noting that not only do the mineral proportions change as a function of depth, the chemical compositions of the mineral phases also vary significantly with depth. Different geotherms were used in our calculations based on their tectonic settings (Artemieva, 2019; Katsura, 2022; Reston & Morgan, 2004). Using the database from Stixrude and Lithgow-Bertelloni (2022), the element K cannot be included in Perple_X calculations. Since K_2O content is relatively low (<1 wt%) in the lower continental crust and the behavior of K is similar to Na in the eclogitic materials at low concentration ($K_2O \sim 0.2$ wt.%) or at lower pressures (<~10 GPa; Agashev et al., 2018; Aoki & Takahashi, 2004; Wang & Takahashi, 1999), we treated all the K as Na in this study. At pressures higher than ~10 GPa, small amount of K-hollandite may form as shown in previous studies on K-rich lithologies ($K_2O > 1.3$ wt.%; e.g., Irifune et al., 1994; Wang & Takahashi, 1999). However, considering the main purpose of this study is to investigate the continental lithosphere (100–200 km depth) and the lack of experimental constraints for the presence of K-hollandite in lithologies with moderate K_2O content (0.4–1.0 wt.%), we did not consider the presence of K-hollandite in this study.

3. Results

3.1. High Pressure-Temperature Single-Crystal Elasticity of Jadeite

We conducted least-squares inversions of the Christoffel equation to obtain the best-fit C_{ij} model and then Vp and Vs at every pressure-temperature condition which were used for deriving the pressure and temperature derivatives of the elastic moduli using temperature-dependent finite-strain equation of state (Text S3 in Supporting Information S1; Davies, 1974; Davies & Dziewonski, 1975; Duffy & Anderson, 1989). Voigt-Reuss-Hill (VRH) averaging scheme was employed to obtain the aggregate elastic properties (Hill, 1963).

During the inversion process, the elastic properties of jadeite at ambient conditions (K_{S0} = 138(3) GPa, G_0 = 84 (2) GPa, and ρ_0 = 3.302(5) g/cm) from Hao et al. (2020) were fixed. The K_S, G, and C_{ij}s at each pressure-temperature condition are then recalculated utilizing the updated densities from the finite strain fitting (Table S2 in Supporting Information S1). Figure S3 in Supporting Information S1 shows the measured velocities at different Chi angles and the velocities predicted from the best-fit C_{ij} model at 16.7(2) GPa 500 K.

Using the experimentally determined thermal expansion coefficient $\alpha_0 = 3.4(5) \times 10^{-5}$ K^{-1} for the same jadeite sample in Hao et al. (2020), the fitting of high pressure-temperature data yields $K_{S0}' = 3.76(5)$, $G_0' = 1.11(2)$, $\partial K_{S0}/\partial T = -0.028(2)$ GPa/K, and $\partial G_0/\partial T = -0.004(1)$ GPa/K with K_{S0} = 138(3) GPa, G_0 = 84(2) GPa, and ρ_0 = 3.302(5) g/cm^3. The K_{S0}' and G_0' determined in this study are consistent with the values reported in Hao et al. (2020) within uncertainties. We also tested two additional fitting approaches: one includes previous high pressure-temperature X-ray diffraction measurements, and the other one excludes the room-temperature high-pressure elasticity data from Hao et al. (2020). Both yield similar results to what were shown above. Details can be found in Texts S4 and S5 in Supporting Information S1. To estimate the uncertainties of the velocities under high pressure-temperature conditions, we used Monte Carlo method. At 4 GPa and 1273 K, which is the approximate pressure-temperature condition at the middle of continental lithosphere, the estimated Vs uncertainty is 66–67 m/s (Text S6 in Supporting Information S1).

Figure 1 shows the measured Vp, Vs, K_S, and G of jadeite under high pressure-temperature conditions. The most interesting feature is the extremely small temperature dependence of G and Vs of jadeite. As a result, at 1700 K in the upper mantle, the Vs of jadeite is much higher than all the other major upper mantle minerals (Figure 1c), including pyrope. Figure S5 in Supporting Information S1 shows all the high pressure-temperature C_{ij}s of jadeite determined in this study. Most of the C_{ij}s increase with pressure and decrease with temperature. The temperature dependences of many C_{ij}s (e.g., C_{55}, C_{66}, and C_{13}, etc.) are very small, which explains the extremely small temperature dependence of G.

3.2. The Compositions and Proportions of the Major Minerals in PDLCC at High Pressure-Temperature Conditions

Figure 2 shows the calculated mineral proportions of the PDLCC under different tectonic settings from 30 to 500 km depth. From the top of the upper mantle down to the middle of the mantle transition zone, clinopyroxene and garnet are always the dominant mineral phases (sum up to ~70–80 vol%) regardless of the tectonic environments. The proportion of silica phases (~10–20 vol%) remains constant throughout the entire upper mantle.

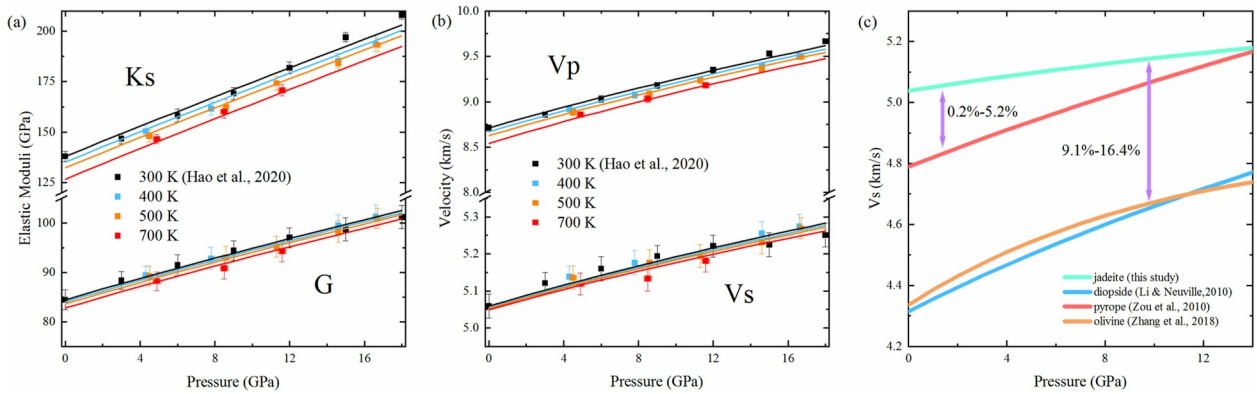

Figure 1. (a, b) The high pressure-temperature aggregate elastic moduli and sound velocities of jadeite. Solid lines are finite strain equation of state fitting results. (c) The Vs of various major upper mantle minerals at 1700 K.

Due to the high Al content in the PDLCC (Rudnick & Fountain, 1995), kyanite (Al_2SiO_5) exists at the top of the upper mantle and gradually dissolves into garnet and/or clinopyroxene at 100–150 km depth. Plagioclase is primarily a crustal phase whose stability field depends on the tectonic environment. After plagioclase dissolves into clinopyroxene at depths of 50–100 km, jadeite becomes the dominant component in clinopyroxene ranging from 50 mol% to 85 mol%. The chemical compositions of clinopyroxene and garnet gradually change with depth as well, as shown in Figure 2.

4. Implications

The potential existence of the PDLCC in the mantle has been supported by geochemical observations in previous studies. For example, the oxygen isotopes of the mantle xenoliths found underneath the North China Craton (NCC) suggest the intracontinental recycling of delaminated crust (e.g., Wang et al., 2018). As explained in the introduction section, we would like to evaluate different hypotheses, in particular the existence of PDLCC, that have been proposed to explain the fast seismic anomalies at 100–200 km depth under continental cratons. Utilizing the calculated mineral proportions/compositions and the experimentally determined elasticity of jadeite and other minerals from previous studies (Table S3 in Supporting Information S1), we calculated the density and seismic velocities of PDLCC under different tectonic environments from 30 to 500 km depth. To estimate the densities and elastic moduli of the multi-phase aggregates, we used the VRH averaging scheme (Text S7 in Supporting Information S1). Since the measurements conducted in this study were limited to 700 K, we estimated the velocity uncertainties propagated from the uncertainties of $\partial K/\partial T$ and $\partial G/\partial T$. They are ~10 m/s for both Vp and Vs at relevant pressure-temperature conditions, which is too small to significantly affect the modeling results (Text S8 in Supporting Information S1).

4.1. 1-D Seismic Properties of PDLCC

As shown in Figure 3, compared to the 1-D seismic model Ak135 or pyrolite model along a cold geotherm, the density of the PDLCC along cold geotherms (active rifts, continental arcs, platform shield, and average) is higher than ambient mantle at depths greater than 40–50 km. This clear density contrast between 40 and 200 km depth makes the thickened continental crust gravitationally unstable. At 200–300 km depth, the density of the PDLCC becomes comparable to the ambient mantle. The Vp of the PDLCC along cold geotherms is similar to, or higher than the Ak135 seismic model at depths greater than ~50 km. At depths of ~50–90 km, ~200–300 km, and ~400–500 km, the Vp of the PDLCC along cold geotherms is similar to ambient upper mantle. However, at depths of ~90–200 km and ~300–410 km, the Vp is higher than the Ak135 seismic model by ~5% and 6%, respectively. The Vs of the PDLCC along cold geotherms is higher than the Ak135 seismic model at depths greater than 40 km. The largest Vs contrast between the PDLCC along cold geotherms and normal mantle exists at 100–200 km depth (~5%–7%) and 300–410 km depth (~7.4%–10.7%). At 300 km depth, due to the coesite to stishovite phase transition, both density and velocities of PDLCC increase significantly (Yang & Wu, 2014).

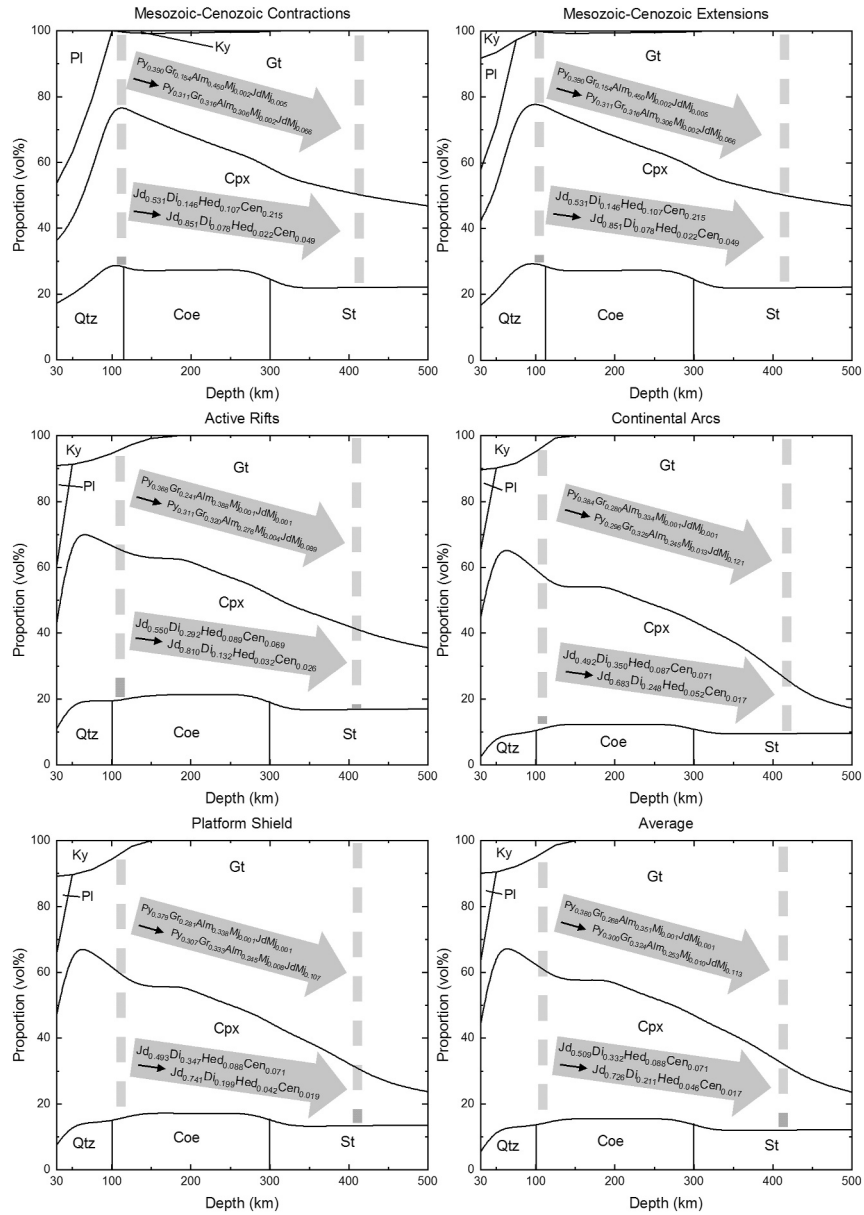

Figure 2. The mineral proportions of the PDLCCs under different tectonic environments calculated using Perple_X. The compositional change of garnet and clinopyroxene between the two gray dashed lines are shown by the gray arrows. At pressures <~10 GPa, the element partitioning behavior of K is similar to Na and mainly exist in Cpx. At pressures >~10 GPa, small amount of K-hollandite may present. (Pl: plagioclase; Ky: kyanite; Gt: garnet; Cpx: clinopyroxene; Qtz: quartz; Coe: coesite; St: stishovite; Jd: jadeite; Di: diopside; Hed: hedenbergite; Cen: clinoenstatite; Py: pyrope; Gr: grossular; Alm: almandine; Mj: majorite; JdMj: jadeite majorite).

4.2. The Fast Seismic Anomalies at 100–200 km Under Continental Cratons

The fast Vs anomalies under continental cratons have been observed globally between 100 and 200 km depth. The SEMum2, GLAD-M25, and DR2020s models all show similar geographic distributions of fast Vs anomalies at ~150 km depth with the highest Vs ranging from ~4.8 km/s to 4.9 km/s (Figure 4a; Figure S6 in Supporting Information S1; Debayle et al., 2020; French et al., 2013; Lei et al., 2020). The discussion below focuses on the GLAS-M25 model, and the results based on the other two models are presented in Text S9 and Figure S6 in Supporting Information S1.

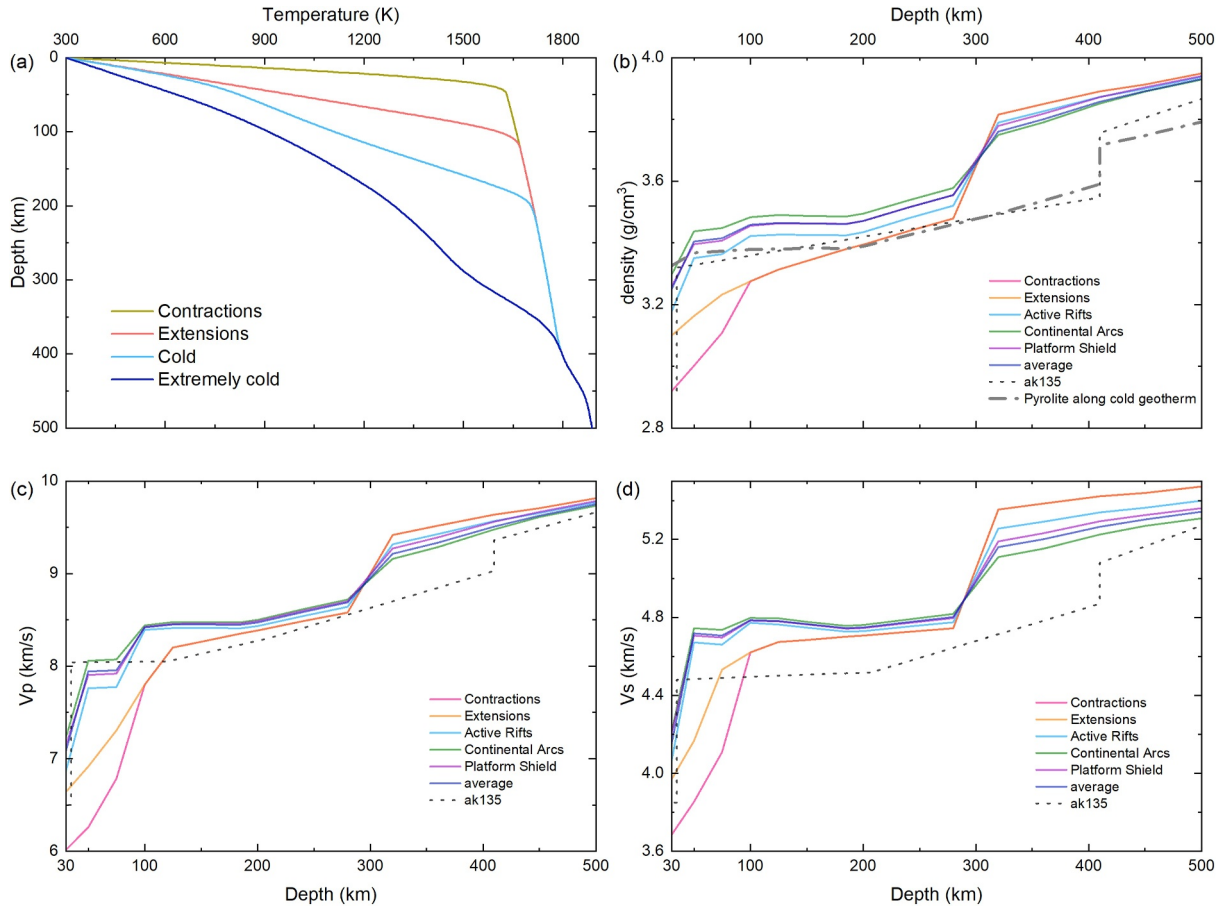

Figure 3. (a) The geotherms used for the Perple_X calculations. The cold geotherm (after Reston & Morgan, 2004) is used for Platform Shield, Continental Arcs, Active Rifts, and average lower continental crust. The extremely cold geotherm and ambient mantle temperature (1600 K adiabat) are adopted from Artemieva (2019) and Katsura (2022). (b–d) are the density, Vp, and Vs of the PDLCCs under different tectonic environments from 30 to 500 km depth, respectively.

To evaluate different hypotheses for explaining the fast Vs anomalies under continental cratons, we calculated the Vs (Voigt bound) of pyrolite, harzburgite, and eclogite at 150 km depth under different temperatures assuming different Mg#s in the constituting mafic minerals (Figure 4b). To be consistent, we used exactly the same method (Perple_X with Stixrude and Lithgow-Bertelloni (2022) thermodynamic database) to calculate the mineral proportions and compositions of pyrolite and harzburgite at different depths. Voigt bound was used since the seismically observed Vs of cratonic lithosphere is actually the Voigt-average isotropic shear wave velocity (French & Romanowicz, 2014; Lei et al., 2020). Pyrolite, harzburgite, and eclogite represent ambient mantle (~60 vol% olivine), olivine-rich lithosphere (~80 vol% olivine), and PDLCC, respectively. The bulk chemical composition of the eclogite here, which represents the PDLCC, is the average lower continental crust chemical composition from Rudnick and Fountain (1995) (Table S1 in Supporting Information S1). Two different temperatures are assumed at 150 km depth under craton: one is 300 K lower than the adiabatic ambient mantle (at ~1400 K) representing cold temperatures expected under the "normal" cratons; the other one is at ~1000 K, which is expected to be seen only under extremely cold cratons (Figure 3a). According to previous mantle xenoliths studies, the Mg# of the mafic minerals can increase from ~89 in the ambient mantle to ~92–93 in the cratonic lithosphere (e.g., Jaques et al., 1990; Kopylova & Russell, 2000). Thus, we considered pyrolite, harzburgite, and eclogite with ~30% less Fe (Mg# ~92.3) compared with the ambient mantle.

As shown in Figure 4b, along normal cold geotherms, even with Mg# as high as 92.3, the Vs of pyrolite/harzburgite could only reach ~4.7 km/s, whereas the Vs of eclogite with ~30% less Fe is higher than 4.8 km/s. Along an extremely cold geotherm (1000 K at 150 km depth), the Vs of pyrolite/harzburgite is ~4.82 km/s, whereas the Vs of eclogite could reach 4.9 km/s. We identified two regions in GLAD-M25 model (Figure 4c): blue regions with Vs higher than 4.82 km/s, which could only be explained by delaminated eclogitic PDLCC and green regions

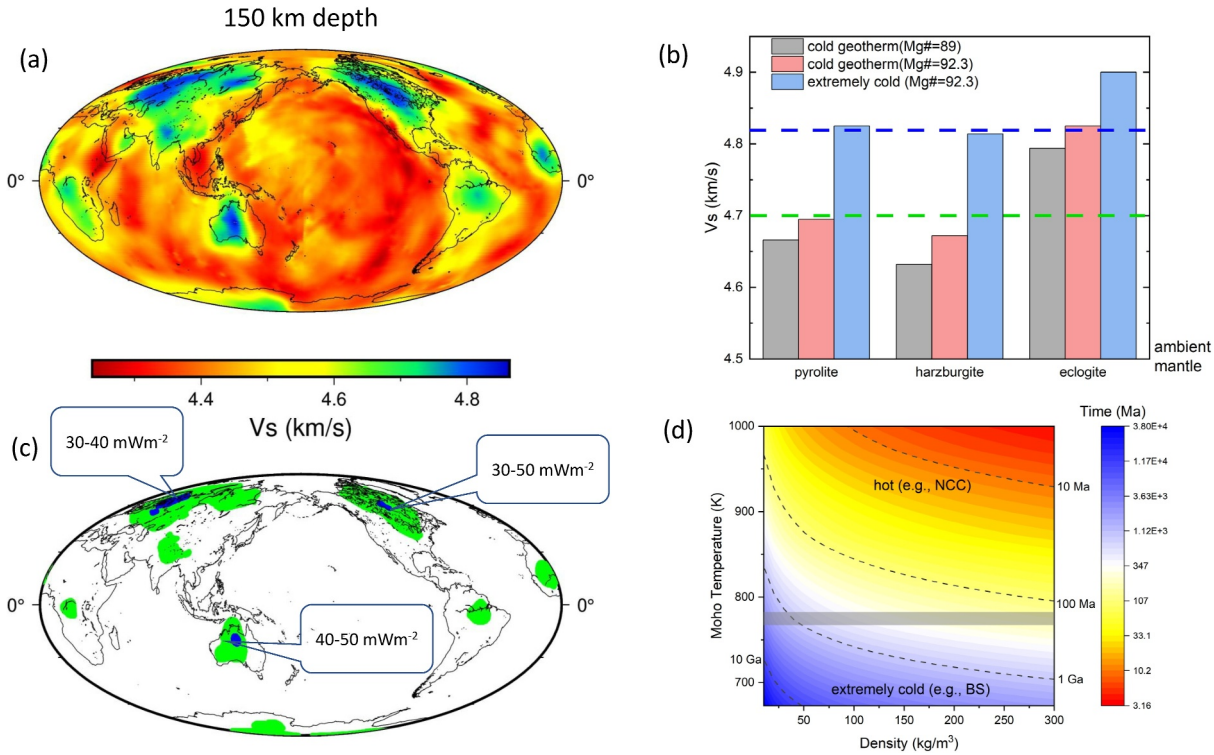

Figure 4. (a) The global Vs map at 150 km depth from the GLAD-M25 model (Lei et al., 2020). (b) The Vs (Voigt bound) of pyrolite, harzburgite, and eclogite with different temperatures and Mg#s. The blue and green dashed lines marked the Vs of 4.82 km/s and 4.7 km/s, respectively. (c) The global distribution of potentially delaminated eclogitic materials based on the global Vs model. Blue and green regions are with Vs > 4.82 km/s and Vs between 4.82 and 4.7 km/s, respectively. The heat flux data are obtained from Mareschal and Jaupart (2013). (d) The critical instability time to initiate the delamination of a 10-km thick eclogitic lower continental crust changes with varying Moho temperature and density contrast, adopted from Jull and Kelemen (2001) and Hacker et al. (2015). The gray line shows the Moho temperature along a regular cold cratonic geotherm. (NCC: North China Craton; BS: Baltic Shield).

with Vs between 4.7 and 4.82 km/s, which could be explained by either the extremely low temperatures and/or the presence of small amounts of PDLCC (e.g., mixing 18% of eclogitic PDLCC with pyrolite/harzburgite is enough to increase the Vs to 4.7 km/s along a normal continental cold geotherm). As shown in Figure 4c, the blue regions only exist in Eastern Canada, Western Australia, and Eastern Europe, where previous xenoliths or petrogenesis studies support potential delamination processes taking place in the past (Kovalenko et al., 2005; Smithies & Champion, 1999; Whalen et al., 2010). The green regions, on the other hand, are widely distributed under different cratons, including Northern North America, Central Southern America, Western Australia, Southern and Northern Asia, Southern and Eastern Africa, and Eastern Europe, suggesting the likelihood of a combination of multiple causes, including chemical depletion, cold temperature, and PDLCC.

Another potential explanation for the fast Vs anomalies under cratons is the presence of a small fraction of diamond. Garber et al. (2018) considered 2 vol% of diamond plus 20 vol% of eclogite as a better explanation since eclogite is not fast enough. However, the Vs of jadeite in Garber et al. (2018) is 0.15–0.35 km/s lower than what was determined in this study (Figure S7 in Supporting Information S1), resulting in an underestimated Vs of eclogite. Utilizing the updated thermoelastic properties of jadeite, the vol.% of eclogite that is needed to increase Vs to 4.7 km/s is less than 18% along a normal continental geotherm (Artemieva, 2019; Reston & Morgan, 2004). In addition, the ultra-small volume fraction of diamond found in the cratonic lithosphere (<0.0001–0.01%; Pearson et al., 2003) makes it difficult to be detected by typical teleseismic waves with ~10–100 km wavelengths. Therefore, based on the elasticity of jadeite determined in this study, the existence of diamond is not required to explain the fast seismic anomalies under craton, although local diamond enrichment may help.

Delamination of lower continental crust has been extensively studied in the past (e.g., Jull & Kelemen, 2001), and it depends on many factors, such as Moho temperature, density contrast, and the thickness of the eclogitic layer. Adopting the crustal delamination model presented in Jull and Kelemen (2001) and Hacker et al. (2015), we

plotted the critical instability time that is needed to initiate the delamination of a 10 km thick dense eclogitic lower continental crust layer as a function of Moho temperature and density contrast (Figure 4d). The Moho temperature has a strong effect on the critical instability time. Under normal cold cratons, the instability time is between 100 Ma to 1 Ga. If the Moho temperature is high (e.g., NCC), the critical instability time can be as short as ~10 Ma or even less. However, if the Moho temperature is extremely low (e.g., Baltic Shield), the instability time increases to >1 Ga, and delamination of the lower continental crust is extremely difficult to occur in geological time. It is worth noting that the critical instability time represents the time that is needed for the lower crust to initiate the delamination. As shown in Figure S8 in Supporting Information S1, the formation and sinking of a "lower crustal drip" takes at least several critical times. It is possible that the cratons were colder or warmer in the past, and delamination might have been more difficult or easier at other times in their geological history. The thermal history of cratons is hard to constrain, and thus we used the present-day heat flux to estimate the current Moho temperatures under cratons and the dynamic stability of lower continental crust (Mareschal & Jaupart, 2013). For example, the high heat flux of NCC (>100 $mW \bullet m^{-2}$) suggests a hot Moho, and short critical instability time on the order of 10 Ma or less. The eclogitic materials under NCC may have already sunk to the deeper part of the Earth, which explains the disappearance of fast Vs anomalies under NCC. On the other hand, the heat flux of Eastern Canada, Western Australia, and Eastern Europe, which are the blue regions in Figure 4c, is ~30–50 $mW \bullet m^{-2}$, suggesting a reasonably cold Moho which yields hundreds of Ma critical instability time. Although the eclogitic lower crust is not gravitationally stable in the lithosphere, it would take billions of years for them to fully peel off and sink into the deeper mantle. Typical cratons are ~1.5–2.5 Ga old. Consequently, we can observe the ongoing sinking process (e.g., 3–11 critical instability time as shown in Figure S8 in Supporting Information S1) in cold continental cratons now at many places over the world. Moreover, the slowly delaminating eclogitic lower continental crust can be mixed with ambient mantle at 100–200 km depth under these cratons, which can increase the actual time that is needed to fully sink down to the deep mantle (>200 km) compared to the estimated time from simplified delamination models similar to what is shown in Figure S8 in Supporting Information S1.

Data Availability Statement

All the data can be found in Mendeley Data Repository (Hao, 2023).

Acknowledgments
This study is supported by NSF EAR 1646527 (JSZ) and 1847707 (JSZ). We thank Sergey Tkachev for the Neon gas loading of the DACs at GSECARS, APS, ANL. The use of the gas-loading system and 13-BM-C beamlines are supported by COMPRES under NSF Cooperative Agreement EAR 1661511, and GSECARS is funded by NSF (EAR 1634415) and Department of Energy (DOE)—(DE-FG02-94ER14466). This research used resources of the APS, a U.S. DOE Office of Science User Facility operated for the DOE Office of Science by ANL under Contract NO. DE-AC02-06CH11357. The X-ray Atlas instrument at the University of Hawaii was funded by NSF Grant EAR 1541516 (PD).

References

Agashev, A. M., Pokhilenko, L. N., Pokhilenko, N. P., & Shchukina, E. V. (2018). Geochemistry of eclogite xenoliths from the Udachnaya Kimberlite Pipe: Section of ancient oceanic crust sampled. *Lithos*, *314*, 187–200. https://doi.org/10.1016/j.lithos.2018.05.027

Aoki, I., & Takahashi, E. (2004). Density of MORB eclogite in the upper mantle. *Physics of the Earth and Planetary Interiors*, *143*, 129–143. https://doi.org/10.1016/j.pepi.2003.10.007

Artemieva, I. M. (2019). Lithosphere structure in Europe from thermal isostasy. *Earth-Science Reviews*, *188*, 454–468. https://doi.org/10.1016/j.earscirev.2018.11.004

Connolly, J. A. D. (2009). The geodynamic equation of state: What and how. *Geochemistry, Geophysics, Geosystems*, *10*(10), Q10014. https://doi.org/10.1029/2009GC002540

Dalton, C. A., & Faul, U. H. (2010). The oceanic and cratonic upper mantle: Clues from joint interpretation of global velocity and attenuation models. *Lithos*, *120*(1–2), 160–172. https://doi.org/10.1016/j.lithos.2010.08.020

Datchi, F., Dewaele, A., Loubeyre, P., Letoullec, R., Le Godec, Y., & Canny, B. (2007). Optical pressure sensors for high-pressure-high-temperature studies in a diamond anvil cell. *High Pressure Research*, *27*(4), 447–463. https://doi.org/10.1080/08957950701659593

Davies, G. F. (1974). Effective elastic moduli under hydrostatic stress—I. Quasi-harmonic theory. *Journal of Physics and Chemistry of Solids*, *35*(11), 1513–1520. https://doi.org/10.1016/S0022-3697(74)80279-9

Davies, G. F., & Dziewonski, A. M. (1975). Homogeneity and constitution of the Earth's lower mantle and outer core. *Physics of the Earth and Planetary Interiors*, *10*(4), 336–343. https://doi.org/10.1016/0031-9201(75)90060-6

Debayle, E., Bodin, T., Durand, S., & Ricard, Y. (2020). Seismic evidence for partial melt below tectonic plates. *Nature*, *586*(7830), 555–559. https://doi.org/10.1038/s41586-020-2809-4

Duffy, T. S., & Anderson, D. L. (1989). Seismic velocities in mantle minerals and the mineralogy of the upper mantle. *Journal of Geophysical Research*, *94*(B2), 1895–1912. https://doi.org/10.1029/jb094ib02p01895

French, S., Lekic, V., & Romanowicz, B. (2013). Waveform tomography reveals channeled flow at the base of the oceanic asthenosphere. *Science*, *342*(6155), 227–230. https://doi.org/10.1126/science.1241514

French, S. W., & Romanowicz, B. A. (2014). Whole-mantle radially anisotropic shear velocity structure from spectral-element waveform tomography. *Geophysical Journal International*, *199*(3), 1303–1327. https://doi.org/10.1093/gji/ggu334

Garber, J. M., Maurya, S., Hernandez, J. A., Duncan, M. S., Zeng, L., Zhang, H. L., et al. (2018). Multidisciplinary constraints on the abundance of diamond and eclogite in the cratonic lithosphere. *Geochemistry, Geophysics, Geosystems*, *19*(7), 2062–2086. https://doi.org/10.1029/2018GC007534

Hacker, B. R., Kelemen, P. B., & Behn, M. D. (2015). Continental lower crust. *Annual Review of Earth and Planetary Sciences*, *43*(1), 167–205. https://doi.org/10.1146/annurev-earth-050212-124117

Hao, M. (2023). Fast seismic anomalies under continents explained by the delaminated lower continental crust—Implications from high pressure-temperature elasticity of jadeite [Dataset]. *Mendeley Data, V1*. https://doi.org/10.17632/t2tmrsppsy.1

Hao, M., Pierotti, C. E., Tkachev, S., Prakapenka, V., & Zhang, J. S. (2019). The single-crystal elastic properties of the jadeite-diopside solid solution and their implications for the composition-dependent seismic properties of eclogite. *American Mineralogist: Journal of Earth and Planetary Materials*, *104*(7), 1016–1021. https://doi.org/10.2138/am-2019-6990

Hao, M., Zhang, J. S., Pierotti, C. E., Zhou, W. Y., Zhang, D., & Dera, P. (2020). The seismically fastest chemical heterogeneity in the Earth's deep upper mantle—Implications from the single-crystal thermoelastic properties of jadeite. *Earth and Planetary Science Letters*, *543*, 116345. https://doi.org/10.1016/j.epsl.2020.116345

Hill, R. (1963). Elastic properties of reinforced solids: Some theoretical principles. *Journal of the Mechanics and Physics of Solids*, *11*(5), 357–372. https://doi.org/10.1016/0022-5096(63)90036-X

Irifune, T., Ringwood, A. E., & Hibberson, W. O. (1994). Subduction of continental crust and terrigenous and pelagic sediments: An experimental study. *Earth and Planetary Science Letters*, *126*(4), 351–368. https://doi.org/10.1016/0012-821X(94)90117-1

James, D. E., Boyd, F. R., Schutt, D., Bell, D. R., & Carlson, R. W. (2004). Xenolith constraints on seismic velocities in the upper mantle beneath southern Africa. *Geochemistry, Geophysics, Geosystems*, *5*(1), Q01002. https://doi.org/10.1029/2003GC000551

Jaques, A. L., O'Neill, H. S. C., Smith, C. B., Moon, J., & Chappell, B. W. (1990). Diamondiferous peridotite xenoliths from the Argyle (AK1) lamproite pipe, Western Australia. *Contributions to Mineralogy and Petrology*, *104*(3), 255–276. https://doi.org/10.1007/BF00321484

Jull, M., & Kelemen, P. Á. (2001). On the conditions for lower crustal convective instability. *Journal of Geophysical Research*, *106*(B4), 6423–6446. https://doi.org/10.1029/2000JB900357

Katsura, T. (2022). A revised adiabatic temperature profile for the mantle. *Journal of Geophysical Research: Solid Earth*, *127*(2), e2021JB023562. https://doi.org/10.1029/2021JB023562

Kawai, K., & Tsuchiya, T. (2010). Ab initio investigation of high-pressure phase relation and elasticity in the NaAlSi2O6 system. *Geophysical Research Letters*, *37*(17), L17302. https://doi.org/10.1029/2010GL044310

Kay, R. W., & Kay, S. M. (1993). Delamination and delamination magmatism. *Tectonophysics*, *219*(1–3), 177–189. https://doi.org/10.1016/0040-1951(93)90295-U

Kopylova, M. G., & Russell, J. K. (2000). Chemical stratification of cratonic lithosphere: Constraints from the Northern Slave craton, Canada. *Earth and Planetary Science Letters*, *181*(1–2), 71–87. https://doi.org/10.1016/S0012-821X(00)00187-4

Kovalenko, A., Clemens, J. D., & Savatenkov, V. (2005). Petrogenetic constraints for the genesis of Archaean sanukitoid suites: Geochemistry and isotopic evidence from Karelia, Baltic Shield. *Lithos*, *79*(1–2), 147–160. https://doi.org/10.1016/j.lithos.2004.05.006

Lee, C. T. A. (2003). Compositional variation of density and seismic velocities in natural peridotites at STP conditions: Implications for seismic imaging of compositional heterogeneities in the upper mantle. *Journal of Geophysical Research*, *108*(B9), 2441. https://doi.org/10.1029/2003JB002413

Lei, W., Ruan, Y., Bozdağ, E., Peter, D., Lefebvre, M., Komatitsch, D., et al. (2020). Global adjoint tomography—Model GLAD-M25. *Geophysical Journal International*, *223*(1), 1–21. https://doi.org/10.1093/gji/ggaa253

Mao, H. K., Xu, J. A., & Bell, P. M. (1986). Calibration of the ruby pressure gauge to 800 kbar under quasi-hydrostatic conditions. *Journal of Geophysical Research*, *91*(B5), 4673–4676. https://doi.org/10.1029/JB091iB05p04673

Mareschal, J. C., & Jaupart, C. (2013). Radiogenic heat production, thermal regime and evolution of continental crust. *Tectonophysics*, *609*, 524–534. https://doi.org/10.1016/j.tecto.2012.12.001

Pearson, D. G., Canil, D., & Shirey, S. B. (2003). Mantle samples included in volcanic rocks: Xenoliths and diamonds. *Treatise on geochemistry*, *2*, 568.

Reston, T. J., & Morgan, J. P. (2004). Continental geotherm and the evolution of rifted margins. *Geology*, *32*(2), 133–136. https://doi.org/10.1130/G19999.1

Rivers, M., Prakapenka, V., Kubo, A., Pullins, C., Holl, C., & Jacobsen, S. (2008). The COMPRES/GSECARS gas-loading system for dia- mond anvil cells at the Advanced Photon Source. *High Pressure Research*, *28*(3), 273–292. https://doi.org/10.1080/08957950802333593

Rudnick, R. L., & Fountain, D. M. (1995). Nature and composition of the continental crust: A lower crustal perspective. *Reviews of Geophysics*, *33*(3), 267–309. https://doi.org/10.1029/95RG01302

Schutt, D. L., & Lesher, C. E. (2006). Effects of melt depletion on the density and seismic velocity of garnet and spinel lherzolite. *Journal of Geophysical Research*, *111*(B5), B05401. https://doi.org/10.1029/2003JB002950

Smithies, R. H., & Champion, D. C. (1999). Late Archaean felsic alkaline igneous rocks in the eastern goldfields, Yilgarn Craton, western Australia: A result of lower crustal delamination? *Journal of the Geological Society*, *156*(3), 561–576. https://doi.org/10.1144/gsjgs.156.3.0561

Stixrude, L., & Lithgow-Bertelloni, C. (2022). Thermal expansivity, heat capacity and bulk modulus of the mantle. *Geophysical Journal International*, *228*(2), 1119–1149. https://doi.org/10.1093/gji/ggab394

Walker, A. M. (2012). The effect of pressure on the elastic properties and seismic anisotropy of diopside and jadeite from atomic scale simulation. *Physics of the Earth and Planetary Interiors*, *192*, 81–89. https://doi.org/10.1016/j.pepi.2011.10.002

Wang, C. G., Xu, W. L., Yang, D. B., Liu, Y. S., Pei, F. P., Li, Q. L., & Zhou, Q. J. (2018). Olivine oxygen isotope evidence for intracontinental recycling of delaminated continental crust. *Geochemistry, Geophysics, Geosystems*, *19*(7), 1913–1924. https://doi.org/10.1029/2017GC007284

Wang, Q., Bagdassarov, N., & Shatsky, V. S. (2016). Origin of high-velocity anomalies beneath the Siberian craton: A fingerprint of multistage magma underplating since the Neoarchean. *Russian Geology and Geophysics*, *57*(5), 713–722. https://doi.org/10.1016/j.rgg.2016.01.016

Wang, W., & Takahashi, E. (1999). Subsolidus and melting experiments of a K-rich basaltic composition to 27 GPa: Implication for the behavior of potassium in the mantle. *American Mineralogist*, *84*(3), 357–361. https://doi.org/10.2138/am-1999-0319

Whalen, J. B., Wodicka, N., Taylor, B. E., & Jackson, G. D. (2010). Cumberland batholith, Trans-Hudson Orogen, Canada: Petrogenesis and implications for Paleoproterozoic crustal and orogenic processes. *Lithos*, *117*(1–4), 99–118. https://doi.org/10.1016/j.lithos.2010.02.008

Yang, R., & Wu, Z. (2014). Elastic properties of stishovite and the CaCl2-type silica at the mantle temperature and pressure: An ab initio investigation. *Earth and Planetary Science Letters*, *404*, 14–21. https://doi.org/10.1016/j.epsl.2014.07.020

References From the Supporting Information

Ackermann, R. J., & Sorrell, C. A. (1974). Thermal expansion and the high–low transformation in quartz. I. High-temperature X-ray studies. *Journal of Applied Crystallography*, *7*(5), 461–467. https://doi.org/10.1107/S0021889874010211

Angel, R. J., Miozzi, F., & Alvaro, M. (2019). Limits to the validity of thermal-pressure equations of state. *Minerals*, *9*(9), 562. https://doi.org/10.3390/min9090562

Arimoto, T., Gréaux, S., Irifune, T., Zhou, C., & Higo, Y. (2015). Sound velocities of $Fe_3Al_2Si3O_{12}$ almandine up to 19 GPa and 1700 K. *Physics of the Earth and Planetary Interiors*, *246*, 1–8. https://doi.org/10.1016/j.pepi.2015.06.004

Brown, J. M., Angel, R. J., & Ross, N. L. (2016). Elasticity of plagioclase feldspars. *Journal of Geophysical Research: Solid Earth*, *121*(2), 663–675. https://doi.org/10.1002/2015JB012736

Carpenter, M. A., & Salje, E. K. (1998). Elastic anomalies in minerals due to structural phase transitions. *European Journal of Mineralogy*, *10*(4), 693–812. https://doi.org/10.1127/ejm/10/4/0693

Chen, T., Liebermann, R. C., Zou, Y., Li, Y., Qi, X., & Li, B. (2017). Tracking silica in Earth's upper mantle using new sound velocity data for coesite to 5.8 GPa and 1073 K. *Geophysical Research Letters*, *44*(15), 7757–7765. https://doi.org/10.1002/2017GL073950

Dera, P., Zhuravlev, K., Prakapenka, V., Rivers, M. L., Finkelstein, G. J., Grubor-Urosevic, O., et al. (2013). High pressure single-crystal micro X-ray diffraction analysis with GSE_ADA/RSV software. *High Pressure Research*, *33*(3), 466–484. https://doi.org/10.1080/08957959.2013.806504

Fei, Y. (1995). Thermal expansion. In T. J. Ahrens (Ed.), *Mineral physics & crystallography: A handbook of physical constants*, *AGU reference shelf* (Vol. 2, pp. 29–44). American Geophysical Union. https://doi.org/10.1029/rf002p0029

Gaida, N. A., Gréaux, S., Kono, Y., Ohfuji, H., Kuwahara, H., Nishiyama, N., et al. (2021). Elasticity of nanocrystalline kyanite at high pressure and temperature from ultrasonic and synchrotron X-ray techniques. *Journal of the American Ceramic Society*, *104*(1), 635–644. https://doi.org/10.1111/jace.17464

Gréaux, S., Zhou, Y., Kono, Y., Yamada, A., Higo, Y., & Irifune, T. (2020). Thermoelastic properties of $K_{0.7}Na_{0.3}AlSi_3O_8$ hollandite and $NaAlSi_2O_6$ jadeite: Implication for the fate of the subducted continental crust in the deep mantle. *Minerals*, *10*(3), 261. https://doi.org/10.3390/min10030261

Gwanmesia, G. D., Wang, L., Heady, A., & Liebermann, R. C. (2014). Elasticity and sound velocities of polycrystalline grossular garnet ($Ca_3Al_2Si3O_{12}$) at simultaneous high pressures and high temperatures. *Physics of the Earth and Planetary Interiors*, *228*, 80–87. https://doi.org/10.1016/j.pepi.2013.09.010

Irifune, T., Higo, Y., Inoue, T., Kono, Y., Ohfuji, H., & Funakoshi, K. (2008). Sound velocities of majorite garnet and the composition of the mantle transition region. *Nature*, *451*(7180), 814–817. https://doi.org/10.1038/nature06551

Isaak, D. G., Ohno, I., & Lee, P. C. (2006). The elastic constants of monoclinic single-crystal chrome-diopside to 1,300 K. *Physics and Chemistry of Minerals*, *32*(10), 691–699. https://doi.org/10.1007/s00269-005-0047-9

Jackson, J. M., Sinogeikin, S. V., & Bass, J. D. (2007). Sound velocities and single-crystal elasticity of orthoenstatite to 1073 K at ambient pressure. *Physics of the Earth and Planetary Interiors*, *161*(1–2), 1–12. https://doi.org/10.1016/j.pepi.2006.11.002

Kandelin, J., & Weidner, D. J. (1988). Elastic properties of hedenbergite. *Journal of Geophysical Research*, *93*(B2), 1063–1072. https://doi.org/10.1029/JB093iB02p01063

Kulik, E., Murzin, V., Kawaguchi, S., Nishiyama, N., & Katsura, T. (2018). Thermal expansion of coesite determined by synchrotron powder X-ray diffraction. *Physics and Chemistry of Minerals*, *45*, 1–9. https://doi.org/10.1007/s00269-018-0969-7

Li, B., & Neuville, D. R. (2010). Elasticity of diopside to 8 GPa and 1073 K and implications for the upper mantle. *Physics of the Earth and Planetary Interiors*, *183*(3–4), 398–403. https://doi.org/10.1016/j.pepi.2010.08.009

Liu, J., Chen, G., Gwanmesia, G. D., & Liebermann, R. C. (2000). Elastic wave velocities of pyrope–majorite garnets (Py62Mj38 and Py50Mj50) to 9 GPa. *Physics of the Earth and Planetary Interiors*, *120*(1–2), 153–163. https://doi.org/10.1016/S0031-9201(00)00152-7

McCarthy, A. C., Downs, R. T., & Thompson, R. M. (2008). Compressibility trends of the clinopyroxenes, and in-situ high-pressure single-crystal X-ray diffraction study of jadeite. *American Mineralogist*, *93*(1), 198–209. https://doi.org/10.2138/am.2008.2521

Mookherjee, M., Mainprice, D., Maheshwari, K., Heinonen, O., Patel, D., & Hariharan, A. (2016). Pressure induced elastic softening in framework aluminosilicate-albite (NaAlSi3O8). *Scientific Reports*, *6*(1), 1–10. https://doi.org/10.1038/srep34815

Nestola, F., Ballaran, T. B., Liebske, C., Bruno, M., & Tribaudino, M. (2006). High-pressure behaviour along the jadeite $NaAlSi_2O_6$–aegirine $NaFeSi_2O_6$ solid solution up to 10 GPa. *Physics and Chemistry of Minerals*, *33*(6), 417–425. https://doi.org/10.1007/s00269-006-0089-7

Nishihara, Y., Nakayama, K., Takahashi, E., Iguchi, T., & Funakoshi, K. Ì. (2005). P-V-T equation of state of stishovite to the mantle transition zone conditions. *Physics and Chemistry of Minerals*, *31*(10), 660–670. https://doi.org/10.1007/s00269-004-0426-7 Núñez-Valdez et al., 2013 Núñez-Valdez, M., Wu, Z., Yu, Y. G., & Wentzcovitch, R. M. (2013). Thermal elasticity of (Fex, Mg1−x) 2SiO4 olivine and wadsleyite. *Geophysical Research Letters*, *40*(2), 290–294. https://doi.org/10.1002/grl.50131

Ohno, I., Harada, K., & Yoshitomi, C. (2006). Temperature variation of elastic constants of quartz across the α-β transition. *Physics and Chemistry of Minerals*, *33*(1), 1–9. https://doi.org/10.1007/s00269-005-0008-3

Posner, E. S., Dera, P., Downs, R. T., Lazarz, J. D., & Irmen, P. (2014). High-pressure single-crystal X-ray diffraction study of jadeite and kosmochlor. *Physics and Chemistry of Minerals*, *41*(9), 695–707. https://doi.org/10.1007/s00269-014-0684-y

Reichmann, H. J., Sinogeikin, S. V., Bass, J. D., & Gasparik, T. (2002). Elastic moduli of Jadeite-Enstatite Majorite. *Geophysical Research Letters*, *29*(19), 42-1–42-4. https://doi.org/10.1029/2002GL015106

Sinogeikin, S. V., & Bass, J. D. (2002). Elasticity of Majorite and a Majorite-Pyrope solid solution to high pressure: Implications for the transition zone. *Geophysical Research Letters*, *29*(2), 4-1–4-4. https://doi.org/10.1029/2001GL013937

Suzuki, I., & Anderson, O. L. (1983). Elasticity and thermal expansion of a natural garnet up to 1000K. *Journal of Physics of the Earth*, *31*(2), 125–138. https://doi.org/10.4294/jpe1952.31.125

Wang, J., Mao, Z., Jiang, F., & Duffy, T. S. (2015). Elasticity of single-crystal quartz to 10 GPa. *Physics and Chemistry of Minerals*, *42*(3), 203–212. https://doi.org/10.1007/s00269-014-0711-z

Zhang, J. S., & Bass, J. D. (2016). Single-crystal elasticity of natural Fe-bearing orthoenstatite across a high-pressure phase transition. *Geophysical Research Letters*, *43*(16), 8473–8481. https://doi.org/10.1002/2016GL069963

Zhang, J. S., Bass, J. D., & Schmandt, B. (2018). The elastic anisotropy change near the 410-km discontinuity: Predictions from single-crystal elasticity measurements of olivine and wadsleyite. *Journal of Geophysical Research: Solid Earth*, *123*(4), 2674–2684. https://doi.org/10.1002/2017JB015339

Zou, Y., Irifune, T., Gréaux, S., Whitaker, M. L., Shinmei, T., Ohfuji, H., et al. (2012). Elasticity and sound velocities of polycrystalline Mg3Al2 (SiO4) 3 garnet up to 20 GPa and 1700 K. *Journal of Applied Physics*, *112*(1). https://doi.org/10.1063/1.4736407